Numerical Simulation of Two-Grid Ion Optics Using a 3D Code

John R. Anderson*, Ira Katz†, Dan Goebel†

Jet Propulsion Laboratory
California Institute of Technology
Pasadena, California

A three-dimensional ion optics code has been developed under NASA's Project Prometheus to model two grid ion optics systems. The code computes the flow of positive ions from the discharge chamber through the ion optics and into the beam downstream of the thruster. The rate at which beam ions interact with background neutral gas to form charge exchange ions is also computed. Charge exchange ion trajectories are computed to determine where they strike the ion optics grid surfaces and to determine the extent of sputter erosion they cause. The code has been used to compute predictions of the erosion pattern and wear rate on the NSTAR ion optics system; the code predicts the shape of the eroded pattern but overestimates the initial wear rate by about 50%. An example of use of the code to estimate the NEXIS thruster accelerator grid life is also presented.

Introduction

The success of the Deep Space One (DS1) technology validation mission [1], has led NASA to baseline ion thrusters as the primary propulsion in many future missions. In addition to the NSTAR xenon ion thruster flown on DS1, 80 XIPS ion thrusters have been flown on commercial communications Boeing satellites [2]. The upcoming DAWN mission [3] plans to use NSTAR ion thrusters for propulsion. NASA's Project Prometheus is considering use of ion thrusters on its first proposed mission, the Jupiter Icy Moons Orbiter (JIMO) [4].

When the DS1 mission ended, after successfully completing its mission to flyby Asteroid Braille and Comet Borrely, the ion thruster had processed over 73 kg of propellant and had accumulated 16,265 hours of operation in space. More ambitious missions, such as the JIMO mission, would require ion thrusters to process over a thousand kilograms of propellant and operating times in the 80,000 hour range.

In order to develop and validate ion thrusters for such missions, a combination of modeling and testing will be used. This paper describes a model designed to capture the physics in a critical ion thruster subsystem, namely the ion optics system. The ion optics subsystem is used to accelerate ionized propellant atoms from the discharge chamber into a high velocity ion beam, thereby producing thrust.

Background

In a conventional ion thruster, illustrated in Figure 1, propellant is introduced into the discharge chamber through a propellant manifold and through the discharge cathode. An arc discharge between the discharge cathode and anode is maintained to ionize propellant (by electron impact) in the discharge chamber. A magnetic field set up by permanent magnets is used to improve the ion production efficiency by increasing the effective path length before electrons are lost to the anode. Propellant ions produced in the discharge chamber flow toward the ion optics where they are accelerated by a potential difference between the grids into a high velocity beam to produce thrust. To prevent the thruster from

*Member Technical Staff, Member AIAA
† Member Section Staff, Member AIAA

Copyright © 2004 by the American Institute of Aeronautics and Astronautics, Inc. The U.S. Government has a royalty-free license to exercise all rights under the copyright claimed herein for Governmental purposes. All other rights are reserved by the copyright owner.

charging to a high potential due to this ejection of ions, electrons must be injected into the beam at the same rate as positive ions; the required electron current is supplied by the neutralizer cathode.

The ion optics consists of two plates with thousands of matching holes used to set up the electric field through which propellant ions are accelerated. The upstream plate (in contact with the discharge plasma) is called the screen grid while the downstream plate is called the accelerator grid. A diagram showing a view looking downstream from the discharge chamber through three aperture pairs of such a system is shown in Figure 2. A cross-sectional view through a single set of holes is shown in Figure 3.

Accelerator grid erosion leads to the primary life-failure mechanism in ion thruster; namely grid aperture enlargement that leads to electron backstreaming. This failure mode was the first life limiting mechanism observed in the over 30,000 hour Extended Life Test (ELT) of the NSTAR ion thruster [5]. After 26,000 hours with about 15,000 hours at the highest throttle level (2.3 kW), the thruster could not be operated at the highest throttle level due to this backstreaming problem caused by grid wear. Accurate modeling of the accelerator hole enlargement is required to understand and mitigate this effect. A secondary failure mode results from accelerator grid erosion due to sputtering of the downstream face of the grid by backstreaming ions. This results in the familiar "pits and groves" erosion pattern on the grid surface, which can lead to structural failure of the grids, and/or electron backstreaming if the erosion penetrates all the way through the grid.

Code Physics

The CEX3D code was developed to solve for potentials and ion trajectories through a two-grid ion optics system. The computational domain, outlined in Figure 2, is a triangular wedge extending from the axis of a hole-pair to the midpoint between two aperture pairs; the wedge angle of 30 degrees is chosen to give the smallest area that can be used to model the two-grid ion optics system. Similar triangle will cover each aperture pair by a combination of reflections and rotations. The computational domain extends from the discharge chamber through the optics system into the beam downstream of the accelerator grid.

Shown in Figure 3 are some typical ion trajectories as the ions travel from the discharge chamber (left) through the optics system and into the beamlet downstream of the grids (right). The beveled shapes on the inner radius of the screen and accelerator grids are an approximate representation of cusps produced during chemical etching of the grids used on the NSTAR and similar thrusters.

The code solves for the potential in the computational domain and then solves for the particle trajectories to obtain the space-charge density. The potential is obtained using a finite element approximation to solve Poisson's equation $\nabla^2\phi = -\frac{\rho}{\varepsilon_0}$ where ϕ is the potential, ρ is the charge density, and ε_0 is the permittivity of free space. The computational domain is broken up into discreet volumes with six nodes that have a triangular shape in the x-y plane and this cross-section remains constant in the axial direction. Integration of the Laplacian over each finite volume element gives the "stiffness matrix" for that element; it is a six-by-six submatrix that is input into the global matrix for the system. The global matrix has 21 entries for each node (each node has a row in the matrix). At boundaries some of entries are placed into the charge vector. The potential is specified on the upstream and downstream boundaries, and the normal electric field is specified to be zero along the axial sides of the triangular computational domain. The charge is assigned to the nodes using the weighting from the finite element shape functions.

Beam ions are approximated with several thousand uniformly spaced particles injected at the upstream boundary of the computational domain. The current per particle is found by dividing the total beam current by the number of particles. To determine the ion trajectory, the electric field at the location of the particle is computed and the particle speed and position is updated using a time step that allows the particle to move about 0.1 times a typical element dimension. The current of particles striking each grid is summed to determine the total grid current. The beam current is determined by summing the currents of the particles reaching the downstream boundary. Ions reaching the axial boundaries are reflected back into the computational domain; by symmetry, ions flowing out of the sides are replaced by ions flowing into the computational domain from the adjacent region.

In addition to beam ions, charge exchange ion production rates and charge exchange trajectories are computed. Erosion of the accelerator grid is caused by these charge exchange ions and the location, kinetic energy, incidence angle and current of each particle is recorded and used to compute erosion rates. Charge exchange ions that strike the downstream surface of the accelerator grid can come from several centimeters downstream of the grid;

therefore, the computations domain is usually set to extend 5 cm downstream of the grids. The current to the accelerator grid was computed for the NSTAR ion thruster operating at full power. The predicted accelerator grid current was 8.4 mA which is about 30% higher than the 6.5 mA measured during the ELT and the NSTAR 8,000 hour long duration test (LDT) [6].

The electron density is computed using the barometric law. The upstream electrons are allowed to reach the plane at the downstream surface of the screen grid; the downstream electrons are allowed to reach the downstream surface of the accelerator grid. Due to adverse potential gradients, the electron density in the remaining computational region should be negligible and it is set to zero in the code.

The code solves for the potential and particle trajectories iteratively. First the Laplace solution for the potentials is obtained; then the particle trajectories are computed based on this potential. A fraction of the total ion density is added to the nodes and the potential is recalculated. With this new potential the trajectories are recomputed and a weighted combination of the old and new ion charge is assigned to each node. This process can be repeated until the code converges.

Code Results

In addition to the three-dimensional CEX3D code a two-dimensional CEX2D code has been developed [7]. Although the three-dimensional code is used to predict accelerator grid aperture wall erosion rates and electron backstreaming voltage, the two-dimensional code is typically used for these calculations because the apertures are cylindrical and the CEX2D code can produce these results more quickly. However, the pits and grooves pattern cannot be modeled with an axis-symmetric code and must be modeled with the three-dimensional CEX3D code. To illustrate the capabilities of the CEX2D and CEX3D codes, comparison of code predictions to NSTAR data and an analysis to predict the life of the NEXIS thruster [8], a candidate for use on the JIMO mission, is presented.

As noted earlier, erosion of the accelerator grid by charge exchange ion sputtering was the major life limiting observed during the ELT of the NSTAR flight spare thruster. Photographs of center holes in the grid at the beginning and the end of the test are shown in Figure 4. Note that the triangles in the end of test picture are patches where the erosion has completely penetrated the grid. Laser profilometry measurements shown in Figure 5 indicate that the grid was nearing structural collapse when the test was stopped.

Figure 6 is a contour plot of erosion rate for the NSTAR ion thruster predicted by CEX3D; two-dimensional and three-dimensional views of the same data are shown. Shown is the region surrounding 3 holes; pits form at the center of the triangle between three holes and grooves run along the webbing between the pits.

The wear rate in the pits and grooves pattern changes as the grid erodes. When the grids are new the surface is flat and all the sputtered material leaves the grid. The wear rate slows after the pits form because some of the sputtered material is redeposited on the pit walls—resulting in a reduction in the net amount of material removed. The CEX3D code, used to model the pits and grooves erosion, does not account for redeposition. Therefore the code can be used to predict initial wear rates but over predicts long term wear rates.

A comparison of the grooves erosion rate predicted by CEX3D and the profile measured on the NSTAR grids at the end of the LDT is shown in Figure 7. The eroded depth is proportional to the erosion rate, so the two curves should have the same shape. The width of the groove, shown in Figure 7, is in good agreement with the prediction although the groove is slightly more V shaped than the code prediction.

The shape of the pits, shown in Figure 8, also agrees with the predictions reasonably well, although the calculated pit erosion rate is about twice the measured rate because redeposition in the pit is not taken into account. The pits are narrower than the prediction, but this may be due—in part—to the measurement being taken slightly off the center of the pits and grooves pattern. As seen in Figure 8, the depth of the groove is less than the 50 μm shown in Figure 7, which suggests that the laser profilometer scan may have been slightly off center. Such a scan would not cross the widest or deepest part of the pits and would show pit width and depth smaller than the maximum.

A comparison of the measured and predicted pit depth as a function of time during the LDT is shown in Figure 9. The long-term erosion rate for the pits around the center hole of the NSTAR accelerator grid was determined from a linear fit to the pit depth obtained during the LDT. The long-term erosion rate of 26.5 μm/khr is approximately twice the initial rate of 50 μm/khr estimated by the slope between 0 and the first data obtained during the LDT at 1464 hours. The CEX3D code predicts an initial erosion rate of 73.5 μm/khr; the pit depth that would result if this rate continued through the LDT is also shown in Figure 9. The predicted depth computations are

conservative because the pits erode more slowly than predicted.

The measured pit depths from the LDT of the NSTAR thruster are also shown in Figure 9. The NSTAR ion optics is made from molybdenum and the pits had eroded through 45% of the grid thickness during the LDT. The nominal predicted final pit depth was computed assuming that the pits erode at the 73.5 μm/khr rate, shown in Figure 9, throughout the entire test. If that had occurred the pits would have worn through the grid during the LDT.

Electron backstreaming calculations were done using the CEX2D code. Charge exchange ions striking the accelerator hole wall cause erosion resulting in aperture enlargement to the point where the voltage available from the accelerator grid power supply can no longer prevent electron backstreaming.

Figure 10 shows a comparison of CEX2D calculated and measured accelerator grid aperture diameter after operating the NSTAR thruster at full power for 8 khrs during the LDT. The code predictions agree with the measured values after the LDT at the peak density conditions encountered at the center of the thruster; however, the code over-predicts the erosion at low plasma densities found at larger radii.

Predictions and measurement of the electron backstreaming voltage as a function of accelerator grid aperture diameter for the NSTAR thruster are shown in Figure 11. The accelerator grid must be biased more negative than the electron backstreaming voltage to prevent electron backstreaming. As seen from the data in Figure 11, the code predictions are conservative; that is the thruster operated at higher voltages without backstreaming than predicted by the code.

Wear rate predictions for the NEXIS thruster were made using the CEX2D and CEX3D codes. Table 1 shows predictions of pit depth for the NEXIS and the NSTAR ion thrusters; in addition the measured pit depths from the LDT of the NSTAR thruster are shown.

The NEXIS thruster grids are made from a carbon-carbon composite material. The predicted erosion rate from CEX3D is based on xenon striking molybdenum. Conversion of the erosion rates for molybdenum and carbon-carbon are done as follows. The rate at which the pit depth changes is determined from $\dot{d} = \frac{j}{e}\frac{Y}{\rho}m$ where $\dot{d}$ is the pit depth increase rate, j is the ion current density, e is the electron charge, Y is the sputter yield of the grid material, ρ is the mass density of the grid material, m is the mass per atom of grid material. Given the pit erosion rate for molybdenum, the pit erosion rate for a carbon grid material is found using

$$\dot{d}_C = \frac{Y_C}{Y_{Mo}}\frac{m_C}{m_{Mo}}\frac{\rho_{Mo}}{\rho_C}\dot{d}_{Mo} .$$

The predicted erosion rate of the pits on the downstream surface of the NEXIS accelerator grid is 73.5 μm/khr, ignoring redeposition effects. It is a coincidence that this rate is the same as that for the NSTAR grids. The energy of the ions striking the grid is higher for the NEXIS thruster but there are fewer ions striking the surface. This occurs because the calculations for the NEXIS thruster assumed the thruster was operating in space where the background gas pressure is zero. The NSTAR calculations were made for the conditions in the chamber where the thruster was tested. The background gas pressure during the test was 4×10^{-6} Torr. The background gas increases the amount of charge-exchange collisions, resulting in higher currents to the accelerator grid.

A worst case predicted final pit depth for the NEXIS thruster was computed. The average energy of ions striking the downstream surface of the NEXIS accelerator grid is 541 eV. At this energy converting the rate from molybdenum to carbon-carbon using the largest sputter yield found in the literature for carbon-carbon (0.32) and the smallest yield for molybdenum (0.64) gives the most conservative (largest) pit erosion rate of 23.5 μm/khr for the NEXIS accelerator grid. Assuming that a NEXIS thruster operates for 80 khrs and that the pits erode at this rate the pit depth at the end of the mission would be 1.88 mm or about 70% of the thickness of the grid. The nominal predicted final pit depth was determined from the nominal sputter yields for molybdenum (0.82) and for carbon-carbon (0.28). For the nominal case the predicted pit depth is 1.28 mm or 47% of the NEXIS accelerator grid thickness.

For hole wall erosion material is assumed to be removed uniformly from the barrel. This gives the most conservative estimate of the minimum hole diameter needed for electron backstreaming calculations. The rate at which mass is removed from the barrel of the accelerator grid aperture, assuming singly charged ions, is determined from $\dot{M} = \frac{j}{e}YmA$ where $\dot{M}$ is the mass removal rate and A is the aperture surface area. The conversion for mass removal rates from molybdenum to carbon is

$$\dot{M}_C = \frac{Y_C}{Y_{Mo}}\frac{m_C}{m_{Mo}}\dot{M}_{Mo} .$$

Table 2 shows a comparison of predicted accelerator grid hole diameter for the NSTAR grids for the LDT.

Also shown in Table 2 are predicted accelerator grid hole diameters for the NEXIS thruster. The NSTAR predictions were made for the thruster operating conditions during the LDT, while the NEXIS predictions are made for a thruster operating in space. As seen from the data in Table 2, the nominal predicted and measured final hole diameters for the NSTAR thruster are in good agreement.

A worst-case NEXIS predicted final hole diameter was also determined. A CEX2D calculation shows that for molybdenum on the NEXIS thruster 10.3 mg/khr is removed from the accelerator grid aperture. The average energy of ions striking the hole wall is 1463 eV. The worst case is found by using the smallest sputter yield for molybdenum (1.6) and the largest yield for carbon-carbon (0.75); the mass removal rate for the NEXIS accelerator grid apertures is 0.6 mg/khr. Assuming the NEXIS thruster operates for 80 khr and erodes at this rate the total mass removed from an aperture is 48.3 mg. At this rate the final aperture diameter for the NEXIS thruster accelerator grid hole is 5.28×10^{-3} m. The electron backstreaming margin predicted by CEX2D at beginning of life for the NEXIS thruster is -146 V and this decreases to -29.5 V for the worst case final aperture diameter of 5.28×10^{-3} m. The nominal predicted final hole diameter for NEXIS was found from the nominal sputter yields for molybdenum (1.93) and the for carbon-carbon (0.7) and is 5.04×10^{-3} m. For the nominal case the predicted electron backstreaming margin is -54.6 V. These values are adequate for the expected JIMO mission life.

Estimated Uncertainty

As noted from the data in Figure 9, the predicted initial erosion rate for the NSTAR accelerator grid pits is about 50% higher than the rate observed experimentally. Uncertainties in the predicted erosion rates are dominated by variations in sputter yield as a function of energy and incidence angle given in the literature. The uncertainties in sputter yield data for molybdenum are discussed; the uncertainties in the sputter yields for carbon are of the same order of magnitude.

Figure 12 shows sputter yields found in the literature [9] for xenon ions striking molybdenum. The solid curve is the fit used to compute the erosion rates in the ion optics codes. At higher energies, sputter yield data from different authors agree within 50% but as the energy decreases sputter yield data vary by as much as 350%. In the energy range contributing to pits and grooves erosion (150 to 250 eV) in the NSTAR thruster the uncertainty in sputter yield is 50% to 150%. The maximum sputter yield values given in the literature are at most a factor of two greater than the curve fit used in the optics calculations.

Another factor contributing to uncertainty in sputter erosion rates is the variation in sputter yield as a function of incidence angle. The data are sparse, but for xenon on molybdenum the sputter yield at grazing incidence can be several times the yield at normal incidence[10]. The relative sputter yield for ions striking the surface at off normal incidence angles is shown in Figure 13. Data for the sputter yield as a function of angle suggest that at energies below 1 keV, the maximum relative sputter yield is about 2 to 2.5 times greater than at normal incidence for xenon on both molybdenum and carbon.

Conclusions

Two-dimensional (CEX2D) and three-dimensional (CEX3D) computer codes to model ion optics systems have been developed at JPL. These codes are used to compute predictions of the operating characteristics of existing ion optics systems and can also be used as tools to aid in the design of new optics systems. The CEX3D code predicts the shape of pits and grooves wear pattern observed on the downstream side of the NSTAR accelerator grid but over predicts the initial erosion rate by about 50%. These codes were used to predict the life of the ion optics for the NEXIS thruster; the analysis indicates that the design is adequate to meet current JIMO mission requirements.

Acknowledgements

The research described in this paper was carried out by the Jet Propulsion Laboratory, California Institute of Technology, under a contract with the National Aeronautics and Space Administration.

References

1. Polk, J. E., Brinza, D., Kakuda, R. Y., Brophy, J. R., Katz, I., Anderson, J. R., Rawlin, V. K., Patterson, M. J., Sovey, J., Hamley, J., "Demonstration of the NSTAR Ion Propulsion System on the Deep Space One Mission," IEPC-2001-075, 27th International Electric Propulsion Conference, Pasadena, CA, October 2001.

2. Goebel, D. M., Martinez-Lavin, M., Bond, T. A., King, A. M., "Performance of XIPS Electric Propulsion in On-orbit Station Keeping of the

Boeing 702 Spacecraft," AIAA-2002-4348, 38th AIAA/ASME/SAE/ASEE Joint Propulsion Conference and Exhibit, Indianapolis, IN, July 2002.

3. Brophy, J. R., Marcucci, M. G., Ganapathi, G. B., Garner, C. E., Henry, M. D., Nakazono, B., Noon, D., "The Ion Propulsion System for Dawn," AIAA-2003-4542, 39th AIAA/ASME/SAE/ASEE Joint Propulsion Conference and Exhibit, Huntsville, AL, July 2003.

4. Project Prometheus Web Site, http://spacescience.nasa.gov/missions/prometheus.htm

5. Sengupta, A., Brophy, J. R., Goodfellow, K. D., "Status of the Extended Life Test of the Deep Space 1 Flight Spare Ion Engine after 30,352 Hours of Operation," AIAA-2003-4558, 39th AIAA/ASME/SAE/ASEE Joint Propulsion Conference and Exhibit, Huntsville, AL, July 2003.

6. Polk, J. E., Anderson, J. R., Brophy, J. R., Rawlin, V. K., Patterson, M. J., Sovey, J., Hamley, J., "An Overview of the Results from an 8200 Hour Wear Test of the NSTAR Ion Thruster," AIAA-99-2446, 35th AIAA/ASME/SAE/ASEE Joint Propulsion Conference and Exhibit, Los Angeles, CA, June 1999.

7. Brophy, J. R., Katz, I., Polk, J. E., Anderson, J. R., "Numerical Simulations of Ion Thruster Accelerator Grid Erosion," AIAA-2002-4261, 38th AIAA/ASME/SAE/ASEE Joint Propulsion Conference and Exhibit, Indianapolis, IN, July 2002.

8. Polk, J. E., Goebel, D., Brophy, J. R., Beatty, J., Monheiser, J., Giles, D., Hobson, D., Wilson, F., Christensen, J., De Pano, M., Hart, S., Ohlinger, W., Hill, D. N., Williams, J., Wilbur, P., Laufer, D. M., Farnell, C., "An Overview of the Nuclear Electric Xenon Ion System (NEXIS) Program," AIAA-2003-4713, 39th AIAA/ASME/SAE/ASEE Joint Propulsion Conference and Exhibit, Huntsville, AL, July 2003.

9. Doerner, R. P., Whyte, D. G., Goebel, D. M., "Sputtering yield measurements during low energy xenon plasma bombardment," *Journal of Applied Physics,* Vol. 93, No. 9, pp. 5816-5823, 1 May 2003.

10. Yamamura, Y., Itikawa, Y., Itoh, N., "Angular Dependence of Sputtering Yields of Monatomic Solids," IPPJ-AM-26, Nagoya University, Japan, June 1983.

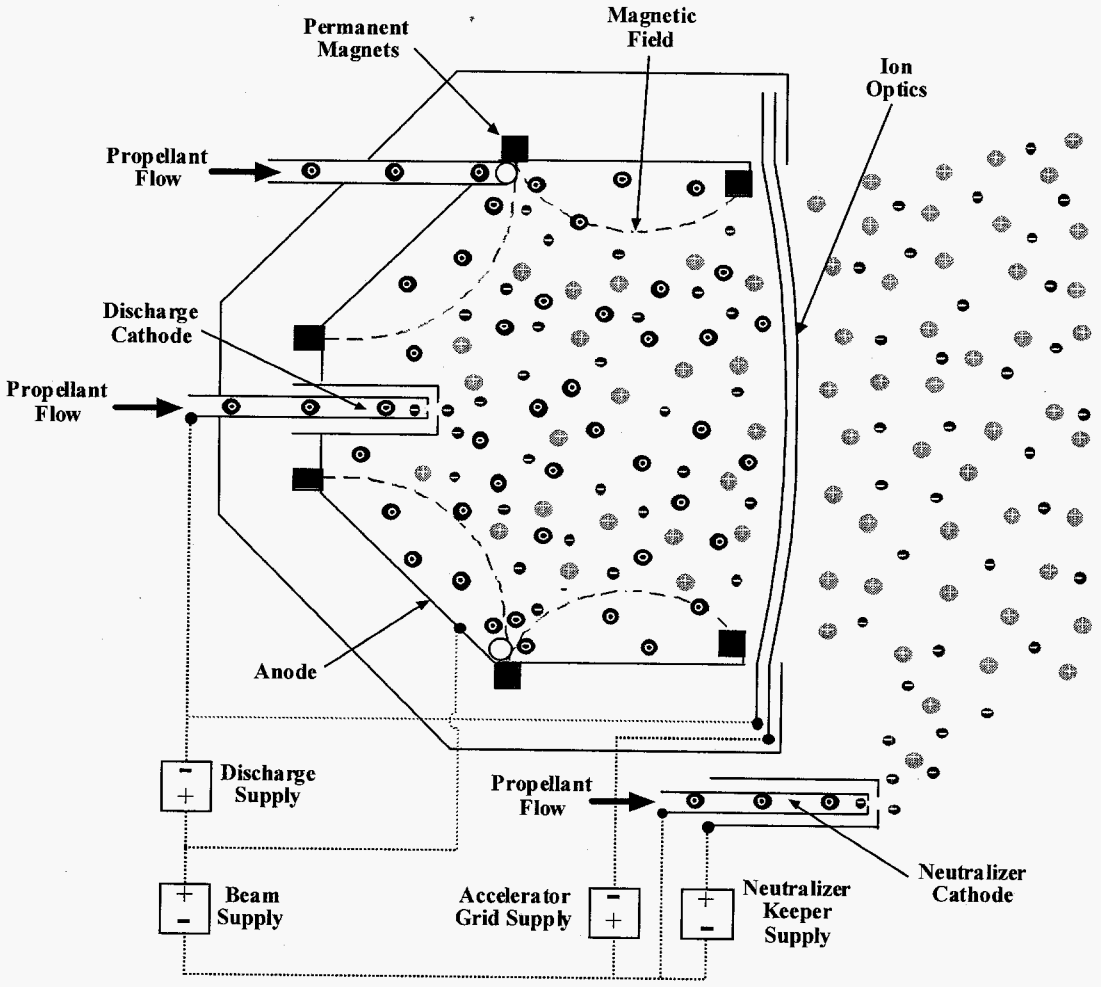

Figure 1. Ion Thruster Schematic

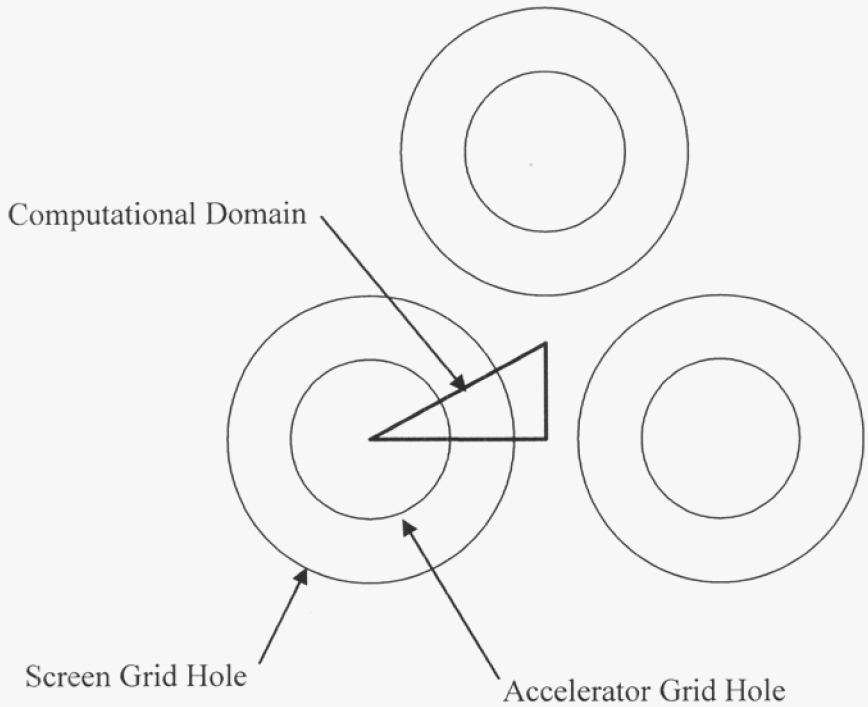

Figure 2. View of Two-Grid Ion Optics System Looking Downstream from Discharge Chamber

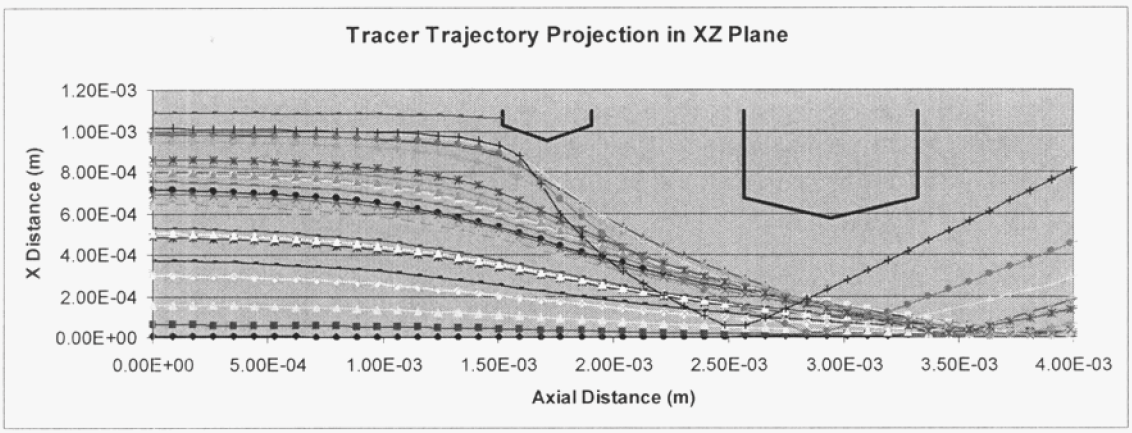

Figure 3. Typical Ion Trajectories

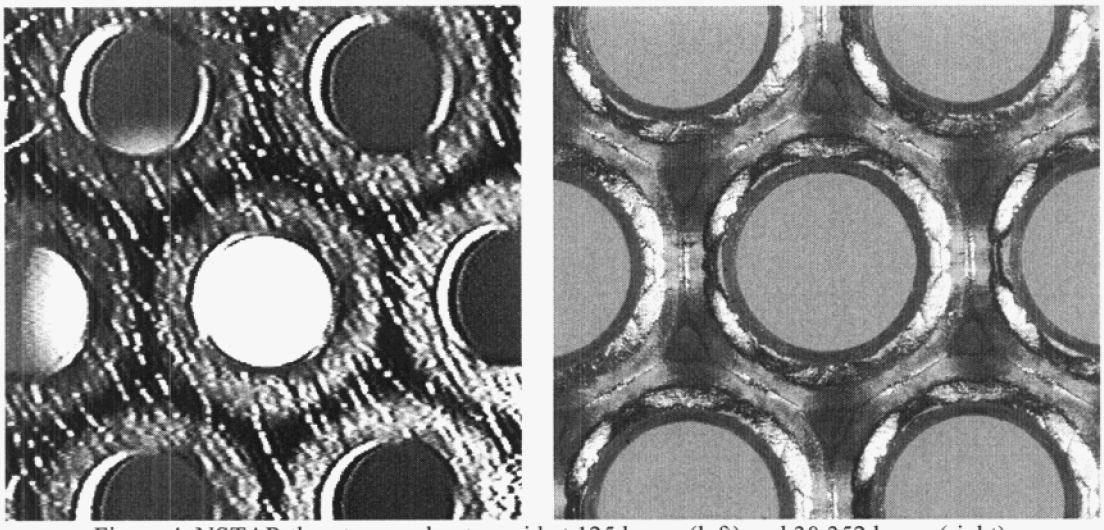

Figure 4. NSTAR thruster accelerator grid at 125 hours (left) and 30,352 hours (right).

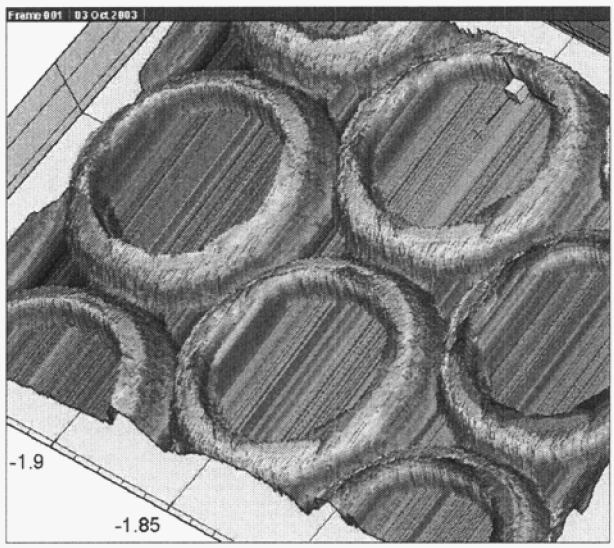

Figure 5. Laser profilometry shows that sputtering in the webbing between the holes had almost destroyed the structural integrity of the NSTAR grids.

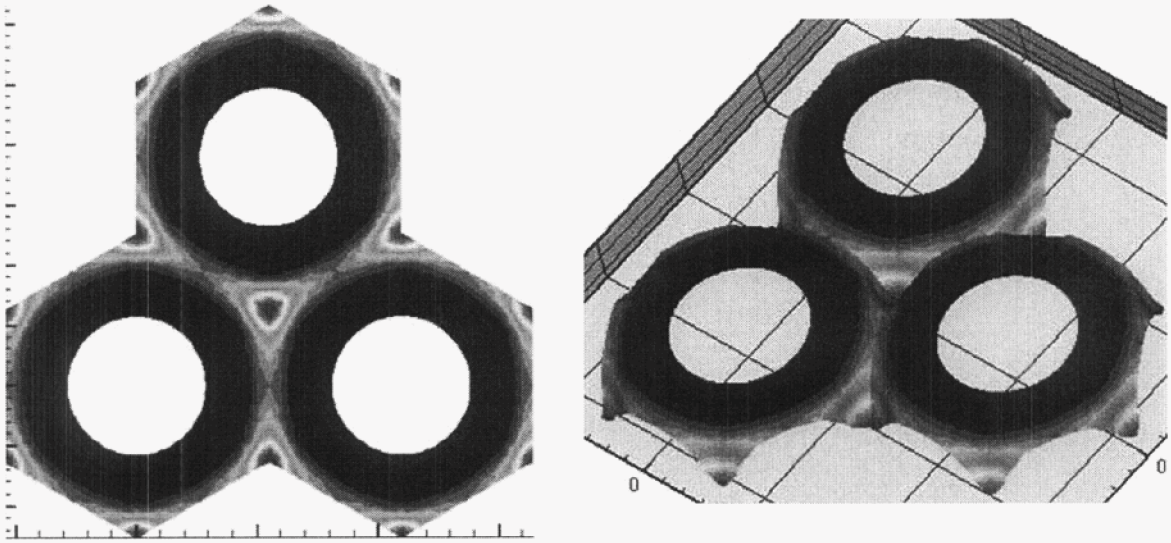

Figure 6. CEX3D Wear Pattern Prediction for NSTAR Thruster

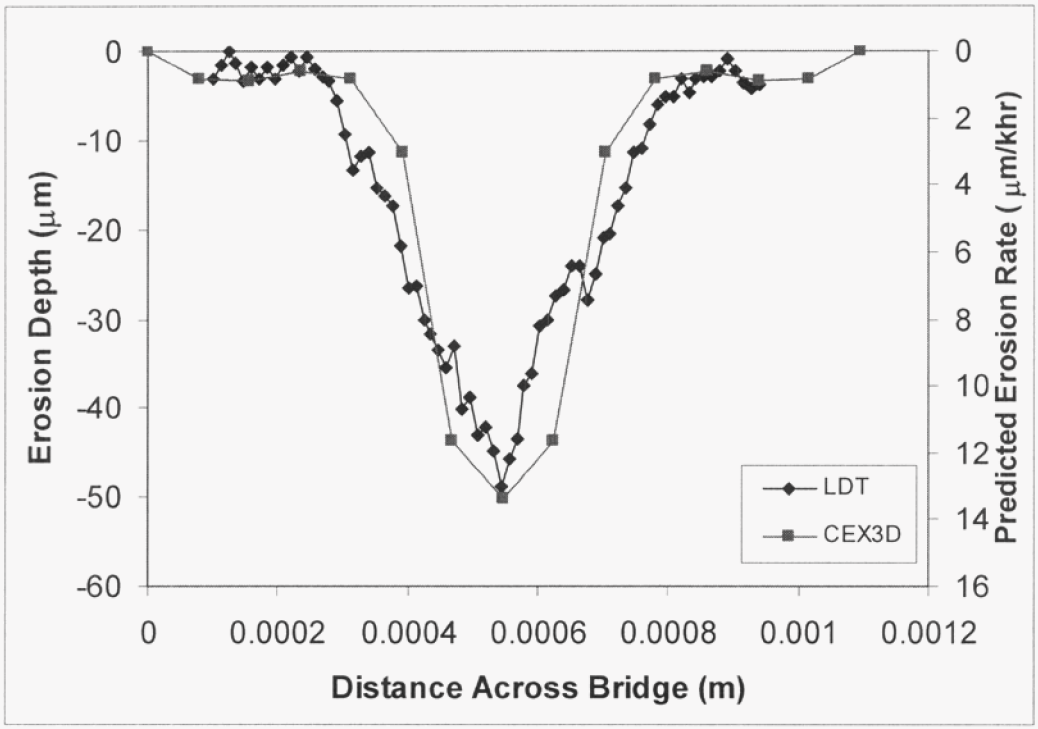

Figure 7. Comparison of Groove Shape After LDT and Predicted Initial Erosion Rate

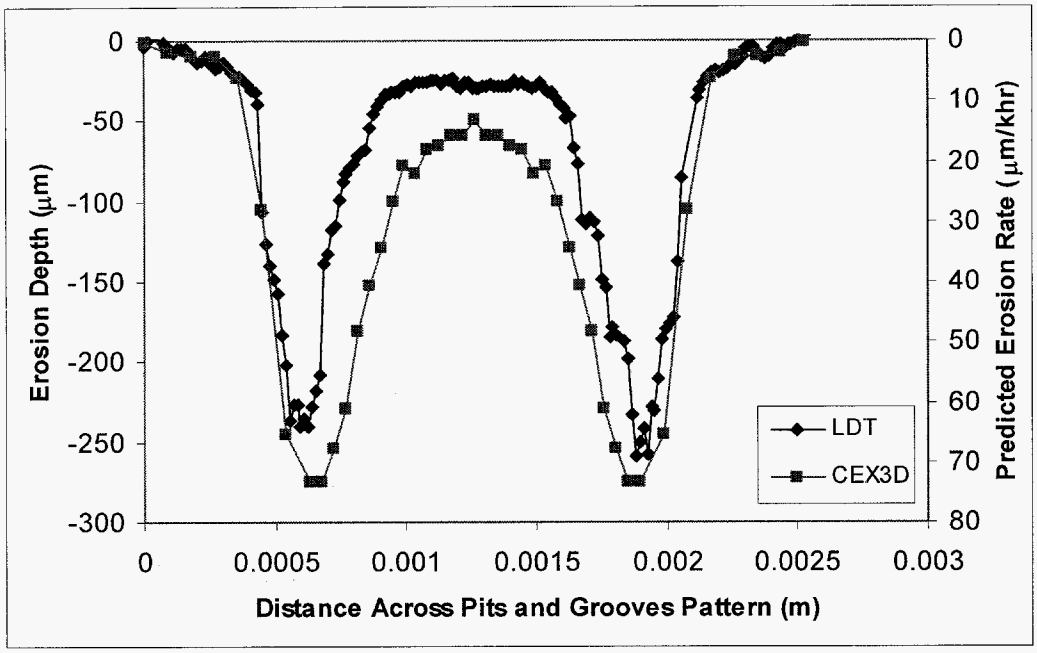

Figure 8. Comparison of Pits and Groove Shape After LDT and Predicted Erosion Rate

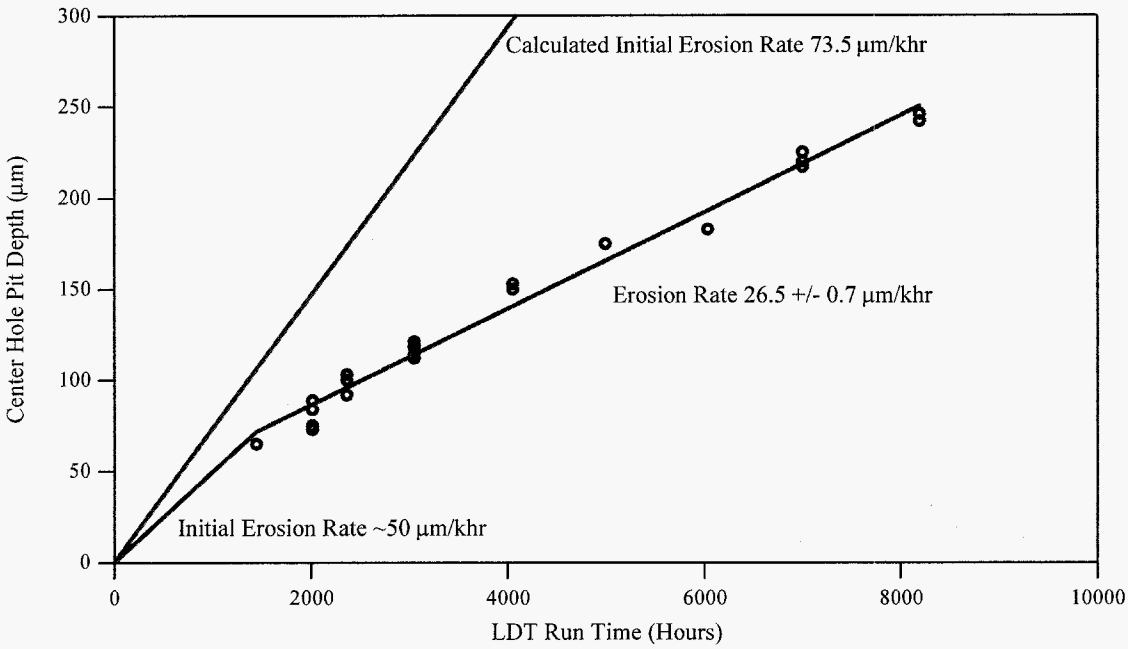

Figure 9. Comparison of Calculated and Measured Pit Depth During LDT

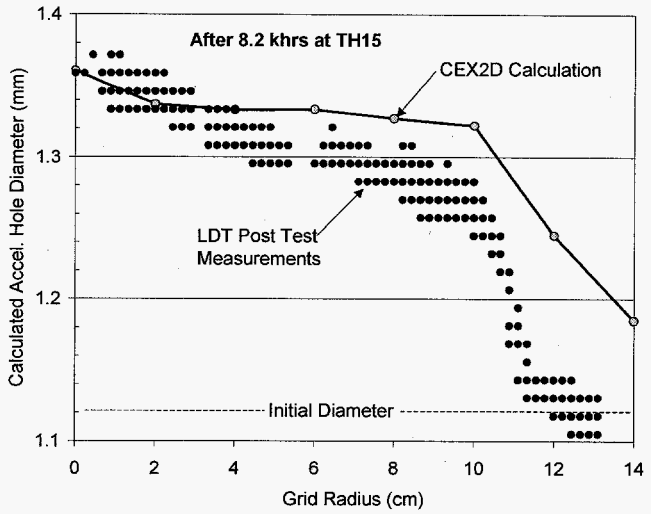

Figure 10. Comparison of Predicted and Measured Hole Diameter After LDT [Figure from Reference 7]

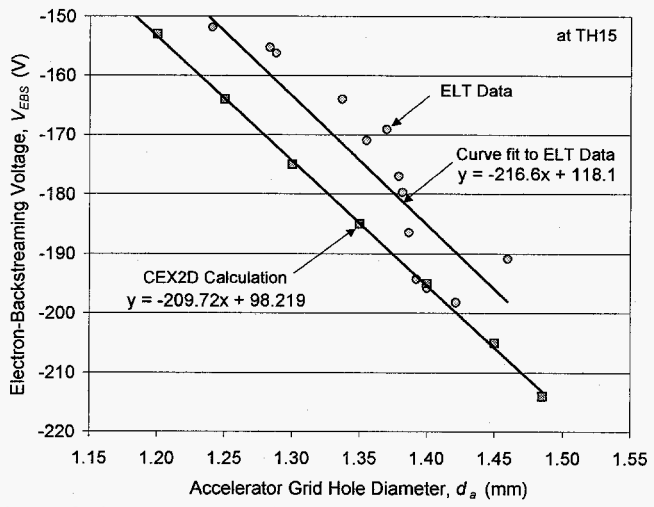

Figure 11. Comparison of Electron Backstreaming Voltage During ELT [Figure from Reference 7]

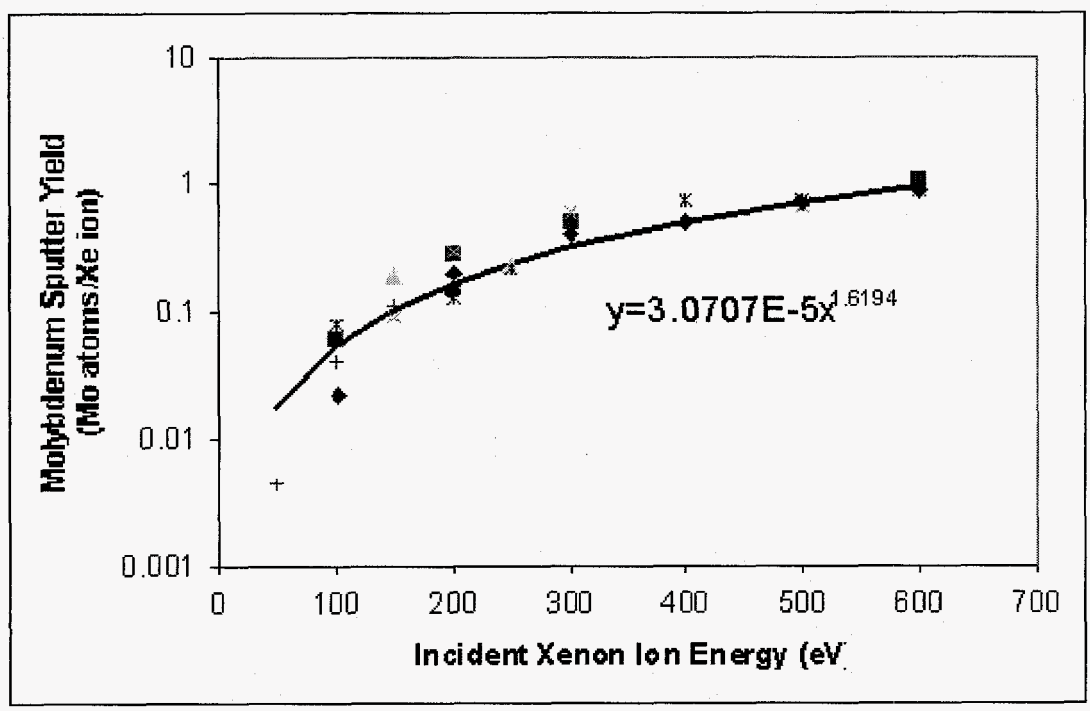

Figure 12. Comparison of sputter yield measurements found in the literature.

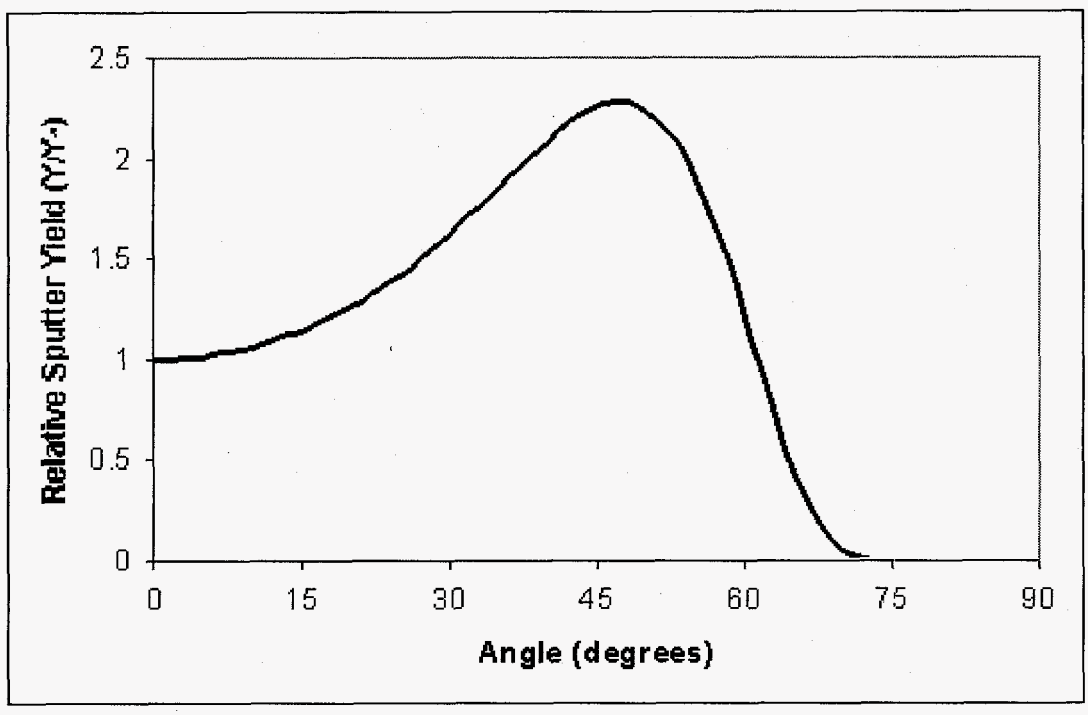

Figure 13. Angular sputter yield relative to normal incidence used in CEX2D and CEX3D.

Thruster	Grid Material	Mission Time (khrs)	Propellant Throughput (kg)	Measured Initial Pit Depth (m)	Measured Final Pit Depth (m)	Nominal Predicted Final Pit Depth (m)	Worst Case Predicted Final Pit Depth (m)	Accelerator Grid Thickness (m)
NSTAR	Molybdenum	8.2	85	0	2.40E-04	6.03E-04		5.07E-04
NEXIS	Carbon-Carbon	80	1670	0		1.28E-03	1.88E-03	2.73E-03

Table 1. Comparison of Pits and Grooves Erosion for NSTAR and NEXIS Thrusters

Thruster	Grid Material	Mission Time (khrs)	Propellant Throughput (kg)	Measured Initial Hole Diameter (m)	Measured Final Hole Diameter (m)	Nominal Predicted Final Hole Diameter (m)	Worst Case Predicted Final Hole Diameter (m)
NSTAR	Molybdenum	8.2	85	1.12E-03	1.36E-03	1.35E-03	
NEXIS	Carbon-Carbon	80	1670	4.08E-03		5.04E-03	5.28E-03

Table 2. Comparison of accelerator grid aperture erosion for NSTAR and NEXIS thrusters